JCI The Journal of Clinical Investigation

Proviral location affects cognate peptide-induced virus production and immune recognition of HIV-1-infected T cell clones

Filippo Dragoni, … , Francesco R. Simonetti, Joel N. Blankson

J Clin Invest. 2023. https://doi.org/10.1172/JCI171097.

Clinical Medicine In-Press Preview AIDS/HIV

Graphical abstract

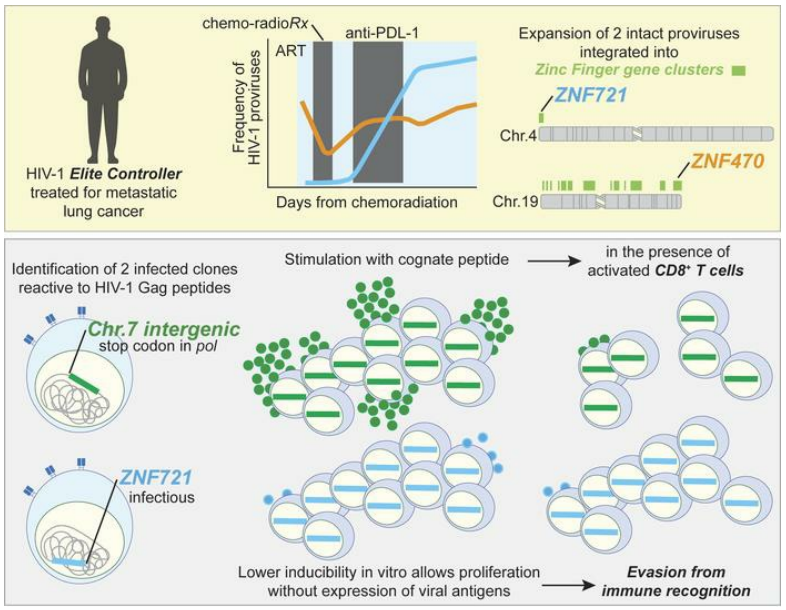

Title

Proviral location affects cognate peptide-induced virus production and immune recognition of HIV-1-infected T cell clones.

Authors

Filippo Dragoni[1], Abena K. Kwaa[1], Caroline C. Traut[1], Rebecca T. Veenhuis[2, 3], Bezawit A. Woldemeskel[1], Angelica Camilo-Contreras[1], Hayley E. Raymond[4#], Arbor G. Dykema[5,6], Eileen P. Scully[1], Amanda M. Rosecrans[1], Kellie N. Smith[5,6], Frederic D. Bushman[4], Francesco R. Simonetti[1,2], and Joel N. Blankson[1,2].

Affiliations

Departments of Medicine (1), Molecular and Comparative Pathobiology (2), Neurology (3), Bloomberg~Kimmel Institute for Cancer Immunotherapy (5), and Sidney Kimmel Comprehensive Cancer Center (6), Johns Hopkins University School of Medicine, Baltimore, MD

Department of Microbiology, University of Pennsylvania, Perelman School of Medicine, Philadelphia, PA (4)

Current Affiliation: Icahn School of Medicine at Mount Sinai

Author list footnotes

Filippo Dragoni and Abena K. Kwaa contributed equally to this work. Francesco R. Simonetti and Joel N. Blankson contributed equally to this work.

Correspondence:

Francesco R. Simonetti, M.D, Ph.D.
Department of Medicine, Johns Hopkins University School of Medicine,
733 N Broadway, Baltimore, MD, 21205, USA.
Phone: 410-955-7757
Email: fsimonetti@jhmi.edu

Joel N. Blankson, M.D, Ph.D.
Department of Medicine, Johns Hopkins University School of Medicine,
855 N Wolfe Street, Baltimore, MD, 21205, USA.
Phone: 410-502-9920
Email: jblanks@jhmi.edu

Conflict-of-interest statement: KNS has filed for patent protection on a subset of the technology described herein (serial No. 16/341,862), has received research funding from AstraZeneca, BMS, Abbvie, and Enara Bio, has received honoraria and speaker fees from Adaptive Biotechnologies, and owns founders' equity in ManaT Bio, Inc.

Abstract

Background. HIV-1-infected $CD4^+$ T cells contribute to latent reservoir persistence by proliferating while avoiding immune recognition. Integration features of intact proviruses in elite controllers (EC) and people on long-term therapy suggests that proviruses in specific chromosomal locations can evade immune surveillance. However, direct evidence of this mechanism is missing.

Methods. In this case report, we characterized integration sites and full genome sequences of expanded T cell clones in an EC before and after chemoradiation. We identified the cognate peptide of infected clones to investigate cell proliferation and virus production induced by T cell activation, and susceptibility to autologous $CD8^+$ T cells.

Results. The proviral landscape was dominated by two large clones with replication-competent proviruses integrated into Zinc Finger genes (*ZNF470* and *ZNF721*) in locations previously associated with deeper latency. A third nearly intact provirus, with a stop codon in Pol, was integrated into an intergenic site. Upon stimulation with cognate Gag peptides, infected clones proliferated extensively and produced virus, but the provirus in *ZNF721* was 200-folds less inducible. While autologous $CD8^+$ T cells decreased the proliferation of cells carrying the intergenic provirus, they had no effect on cells with the provirus in the *ZNF721* gene.

Conclusions. We provide direct evidence that upon activation of infected clones by cognate antigen, the lower inducibility of intact proviruses in ZNF genes can result in immune evasion and persistence.

Funding. Office of the NIH Director and National Institute of Dental & Craniofacial Research; NIAID, NIH; Johns Hopkins University Center for AIDS Research.

Introduction

Shortly after transmission, HIV-1 infection establishes a persistent reservoir of latently infected $CD4^+$ T cells (1-4). Although antiretroviral therapy halts viral replication and prevents disease progression, the long half-life of HIV-1 reservoir cells ($>t_{1/2}$ ~44 months) results in viral rebound upon treatment interruption in most individuals (5, 6). Elite controllers (EC) can spontaneously restrict viral replication in the absence of antiretroviral therapy (ART) due to highly functional cytolytic immune responses that rapidly clear productively infected cells, resulting in undetectable viral loads (7-9). These individuals (<1% of PLWH), represent the ultimate goal of therapeutic strategies aimed at HIV-1 remission (10, 11).

In people on ART and ECs, reservoir stability is mostly caused by the proliferation of infected cells, which undergo clonal expansion beginning in the earliest stages of HIV-1 infection, driven by encounter with cognate antigens and survival stimuli (IL-2, IL-7, IL-15) (12-21). In addition, HIV-1 integration into a handful of specific genes causes insertional mutagenesis, providing a survival advantage (22, 23). Thus, therapeutic strategies that disrupt the proliferation of infected cells would significantly accelerate reservoir decay, contributing to the success of future curative interventions (24). However, cytoreductive and anti-proliferative compounds tested so far failed to significantly reduce reservoir size; moreover, current knowledge of the impact of anti-proliferative drugs on the heterogenous population of HIV-1-infected clones persisting on ART is limited (25, 26).

The proviral landscape is dynamic, shaped by selective forces imposed by HIV-1-host interactions. Growing evidence suggests that HIV-1 integration into chromosomal locations associated with deeper latency are positively selected over time in both EC and PLWH on ART (18, 27, 28). Such genomic regions include centromeric and peri-centromeric repeats, lamina-associate domains (LADs), and the Zinc Finger (ZNF) gene family. Recent studies suggest that intact proviruses integrated into certain ZNF genes, often recurring across individuals, have a

survival advantage due to reduced viral expression caused by the repressive epigenetic environment typical of ZNF gene clusters found in heterochromatic regions (29, 30). However, direct evidence for this mechanism, and whether it affects latency reversal upon physiological stimulation, is lacking. ZNF genes and other repressive genomic locations have been linked to a survival advantage and deeper latency of intact proviruses. In a study from Halvas and colleagues, two proviruses located in *ZNF721/ABCA11P* could be recovered from viral outgrowth and one contributed to persistent nonsuppressible viremia (31). This signature for reservoir selection was first identified in EC, likely due to the strong CTL pressure that selects against proviruses with higher transcriptional activity (18, 27). Similarly, more recent studies in people on ART found a progressive enrichment over time of intact proviruses located in these epigenetically repressed regions(28, 29). Whether these proviruses are permanently “blocked and locked”, and the clinical consequences, remain unclear.

In this study, we characterized HIV-1 persistence in an HLA-B*57^{+} EC before and after treatment with ART, chemoradiation, and anti-PDL-1 immunotherapy for metastatic lung cancer. We performed longitudinal integration site analysis and quantified intact and total HIV-1 DNA by digital PCR. We also assessed the clonal dynamics of two intact proviruses integrated into ZNF genes that, by the end of treatment, dominated the reservoir. Finally, by PBMC stimulation experiments, we resolved the T cell specificity at the epitope level of two infected clones, which allowed us to dissect cell proliferation and provirus inducibility upon peptide-MHC class II recognition, and the impact of immune recognition by autologous CD8^{+} T cells.

Results

Chemoradiation induces a transient contraction of HIV-1 infected cells. The study participant, here referred to as ES24, is a previously described HLA-B*57^{+} male elite controller who maintained undetectable HIV-1 RNA without treatment for more than 10 years (15). In 2019, he was diagnosed with metastatic lung cancer for which he initiated ART and was treated with surgery and a cycle of 5 weekly doses of carboplatin and paclitaxel chemotherapy with radiotherapy (chemoradiation therapy or CRT). This was followed by a 12-month course of immunotherapy with 12 cycles of anti-PD-L1 monoclonal antibody treatment (durvalumab, additional details on his clinical history are provided in Figure 1A). Of note, CD4^{+} T cells reached a nadir on day 67 post CRT (304 cells/μL, 28.8%) and partially recovered by the end of study (643 cells/μL, 30.4%, at day 974). To investigate the impact of treatment on reservoir dynamics, we measured total and intact HIV-1 DNA longitudinally before, during and after CRT (Figure 1A). We observed a rapid but transient decline in both total and intact DNA (2.2- and 3.0- fold reduction, respectively) at 1 month post CRT that coincided with CD4^{+} T cell count nadir (2.3-fold reduction). However, HIV-1 DNA increased in the months after treatment, with a rebound from nadir that was markedly higher for intact DNA (3- versus 9.4-fold for total and intact DNA, respectively), which reached higher levels than pre-CRT (663 versus 82 copies/10^{6} CD4^{+} T cells). Interestingly, single genome sequencing of proviral DNA and outgrowth virus showed a single dominant variant that did not evolve during the study period (Figure 1B), suggesting that the persistence of reservoir cells was driven by cell survival and proliferation, rather than low-level replication, also reflected by the persistently undetectable viral load in plasma. Thus, to further characterize changes in infected cell composition we performed integration site analysis (Figure 1C), which revealed a transient contraction in clonality during CD4 nadir (Gini index 0.41, 0.03, 0.58 at day -624, 151, and 594, respectively). Of note, some integration sites were detected at multiple timepoints, including a provirus found in the *ZNF721* gene, which underwent significant expansion from day

78 to day 594 ($p<0.0001$). Finally, we observed a similar clonal contraction in all $CD4^+$ T cells, measured by TCR sequencing, which preferentially affected the most abundant clones (Figure 1D), as previously described (32). Overall, these result show that although CRT perturbed the frequency and composition of infected cells, reservoir size rebounded upon $CD4^+$ T cell recovery, as recently reported in the context of immunosuppressive therapy post-kidney transplant (33).

Clonal replacement of two intact proviruses integrated into ZNF genes. The sequencing and integration site data suggested that the increase in reservoir size was due to relatively few clones undergoing proliferation, so we sought to determine the genomic integration sites and full genome sequences of infectious proviruses (Figure 2A). We designed primers in the human genome, paired with primers in HIV-1 *gag*, to screen candidate integration sites from day 529, and identified two proviruses integrated into the *ZNF721/ABCA11P* and *ZNF470* genes, termed ZNF721i and ZNF470i going forward, that were genetically intact and matched the *nef* region sequenced from previous time points. ZNF470i was identical to the near full-length sequences of viral outgrowth variants recovered from day -624, while ZNF721i differed only by 2 nucleotides (Figure 2B). These two ZNF genes are located in chromosomes 4 and 19, respectively, both within ZNF gene clusters where intact proviruses have been previously reported from both EC and people on long-term ART (Figure 2C and Supplemental Table S1) (18, 29, 34-36). To investigate the temporal dynamics of these two intact proviruses we quantified their frequencies by integration site-specific digital PCR, and their relative abundance among all infected cells, as recently described (37, 38) (see methods and Figure 2D and E). Total LTR copies and ZNF470i decreased upon CRT initiation and returned to baseline levels; in contrast, ZNF721i underwent significant proliferation and reached a frequency of 741±48 copies/10^6 $CD4^+$ T cells, corresponding to a 69-fold increase from its nadir on day -6 (11±5 copies/10^6 cells) ($p= 0.0001$, Figures 2E and F). At day 1000 post CRT initiation, ZNF721i and ZNF470i together represented more than 80% of all LTR copies, with estimated total-body clone sizes of 120 and 52 million cells, respectively. Together, our results

show that these two intact proviruses found in ZNF genes persisted despite profound perturbation of the HIV-1 reservoir and, in the case of ZNF721i, underwent extensive clonal selection.

Infected clones are common among cells reactive to HIV-1 antigens. To investigate the role of antigen-driven selection of infected cells in ES24, we stimulated CD8-depleted PBMCs, in the presence of antiretrovirals, with CMV and HIV-1 antigens (Figure 3), which have been involved in the persistence of HIV-1-infected clones (39-43). Stimulation of PBMCs with a Gag peptide pool led to a significant increase in LTR DNA copies at 9-days (23.6-fold increase, p=0.01, Figure 3A-C). To determine which proviruses expanded in culture and produced virus, we sequenced the 5'-leader-*gag* region from virion-associated RNA (Figure 3D). We found that 15% of sequences from cells stimulated with Gag peptides matched ZNF721i, while the remaining identified a new variant, markedly different from ZNF721i and ZNF470i, that we did not identify before from proviral DNA or QVOA. This new provirus is nearly intact but shows a premature stop codon in Pol (S311→stop). In addition, it is characterized by a 11-nucleotide deletion within the primer binding site (PBS) hairpin, located in the spacer region between the primer activation sequence and the tRNA annealing region (44) (Figure 3D and E). The provirus (named Chr7.d11sc because of its features) is located in chromosome 7p12.1, in an intergenic region distinct from those previously associated with deeper latency (30). To investigate the presence of specific histone modifications, we interrogated publicly available CHIP-seq data from $CD4^+$ T cells (45); while ZNF721i and ZNF470i were surrounded by epigenetic signatures typical of heterochromatin and ZNF genes (H3K9me3 and H3K36me3), Chr7.d11sc was distant from activating epigenetic marks and showed little enrichment for heterochromatin (Supplemental Figure S1).

To confirm whether the cells carrying this Chr7.d11sc respond to Gag peptide stimulation, we exploited its unique 11-nucleotide deletion to design an assay based on competition probes that would distinguish it from other variants in both genomic DNA and virion-associated RNA (Figure 3F). While ZNF470i did not proliferate in response to antigenic stimulation, we found that

exposure to Gag peptides led to virus production and clonal expansion of both ZNF721i and Chr7.d11sc (32- and >6-fold increase, respectively) (Figure 3G and H). When we compared proviral copies and virus released at the end of culture, we noted that ZNF721i produced less virus despite the extensive proliferation (~10^3 copies/mL, ~10^4 copies/10^6 cells, respectively).

To further characterize these three proviruses of interest, we measured their frequency by integration site specific PCR and performed the qVOA from $CD4^+$ T cells obtained at day 1400 post CRT (Supplemental Figure S2). Out of 5 wells with viral outgrowth (corresponding to 1.44 IUPM), 3 had virus matching ZNF470i and 2 wells had virus matching ZNF721i, demonstrating that these two proviruses are infectious and inducible despite being located within ZNF genes. However, based on the high number of ZNF470i and ZNF721i proviruses screened in the qVOA (961 and 1490), we estimated that less than 0.3% (0.9-0.08%, 95% CI) of proviruses were induced and resulted in outgrowth in vitro (Supplemental Figure S2). In addition, we quantified cell-associated HIV-1 RNA isolated from total $CD4^+$ T cells divided in small aliquots so that they would contain only 1 HIV-1 RNA producing cells, as previously described (46). We detected low-level U5-PBS RNA (average of 11 copies/10^6 cells) and recovered a single U5-gag unspliced RNA sequence, which matched ZNF470i. Taken together, these results confirm the low spontaneous transcriptional activity of ZNF721i and ZNF470i in circulating cells, in vivo (Supplemental Figure S2).

Finally, we repeated the CD8-depleted PBMC stimulation with individual Gag peptides that induced responses by ELISpot and observed increased LTR copies in response to six out of nine peptides (Supplemental Figure S3). Although these proviruses were defective by IPDA (data not shown), our results suggested that HIV-1-reactive $CD4^+$ T cells carrying proviruses are common in this study participant.

Differential inducibility of two proviruses in cells reactive to specific Gag epitopes. To extend our results, we sought to identify the Gag specificity of the clones carrying Chr7.d11sc and

ZNF721i at the epitope level, so that we could investigate proviral inducibility upon encounter with their cognate antigen (Figure 4). As a read out for T cell response to pooled or individual Gag peptides, we used both virus production in the supernatant and infected-cell proliferation (Figure 4A-E, see methods). With this approach we found that the clone harboring Chr7.d11sc is reactive to two overlapping peptides, EKAFSPEVIPMFSAL (41, Gag 162-176) and SPEVIPMFSALSEGA (42, Gag 166-180), while cells harboring ZNF721i respond to STLQEQIGWMTNNPP (61, Gag 241-255). Conversely, ZNF470i did not proliferate or produce virus upon Gag pool stimulation (Supplemental Figure S4). Since the Chr7d11sc provirus is rare and can be detected only in cells after stimulation with peptides 41 and 42, the precise fold increase cannot be quantified; however, we can estimate a minimum of 15- to 20-fold increase using the limit of detection in untreated cells (4 copies/10^6 cells). In subsequent experiments we isolated $CD4^+$ T cells at the end of culture, which confirmed that in the no treatment condition, the frequency of Chr7.d11sc is 2.4±3.3 copies/10^6 $CD4^+$ T cells. Upon stimulation with peptide 61, the frequency of ZNF721i showed a 73-fold increase relative to no treatment. The stimulation with individual cognate peptides is reproducible, as shown by comparable virus production and cell expansion in triplicate experiments (Figure 4D and E, Supplemental Figure S5). In addition, we confirmed that peptides 41, 42, and 61 are recognized by $CD4^+$ T cells, based on the increase in cells positive for intracellular TNFα and IFNγ after 9 days of culture (Figure 4F). Interestingly, 41 and 61 are also recognized by $CD8^+$ T cells (Supplemental Figure S6); indeed, they overlap with well characterized epitopes binding to HLA-B*57 (KAFSPEVIPMF and TSTLQEQIGW, respectively)(47).

We hypothesized that the striking expansion of ZNF721i in vivo and its extensive proliferation ex vivo upon antigen-recognition, are favored by its chromosomal location, allowing proliferation to occur without the cytopathic effects of viral replication. To test this hypothesis, we estimated the proviral inducibility in vitro of ZNF721i and Chr7.d11sc by dividing the copies of

viral RNA in the supernatant by the provirus frequency in cells at the end of culture (Figure 4G). We found that the inducibility in vitro of ZNF721i was almost 200-fold lower (average 57 versus 0.3, p=0.021). Lastly, we used bulk TCRβ sequencing, VDJ-specific dPCR, and combinatorial statistics to identify CASSLTGGGEQFF as the putative CDR3β sequence of the clonotype carrying ZNF721i (Figure 4H and I). CASSLTGGGEQFF had a relative abundance of 0.01% in untreated cells but was among the most abundant clonotypes upon stimulation with peptide 61 (1.8%, test for differential abundance $p<10^{-5}$). Based on provirus and VDJ specific quantification in PBMCs stimulated with peptide 61 and the unstimulated control, we estimated that almost 100% of the clonotype carries ZNF721i, suggesting that most of its clonal selection occurred post HIV-1 integration (Figure 4I and Supplemental Figure S7) (20).

Proliferation of cells harboring ZNF721i is not affected by autologous CD8$^+$ T cells. Clonal expansion of infected clones is the result of opposing forces, such as the frequency of cell stimulation, proliferation rate, and cell death due to viral cytopathic effects. However, immune recognition by cytotoxic cells imposes a major selective force in shaping reservoir dynamics and composition, especially in ECs, resulting in the observed differential genomic distribution of intact proviruses (18, 27). Thus, we sought to determine whether lower proviral inducibility allows infected clones to escape immune recognition. Analysis of Gag and Nef amino acid sequences revealed that Chr7.d11sc had more escape mutations in known B*57-restricted epitopes than ZNF470i and ZNF721i (Figure 5A and Supplemental Figure S8 and S9), suggesting a lower susceptibility to CD8-mediated killing for cells carrying Chr7.d11sc. PBMCs were stimulated for seven days with overlapping peptides covering the entire Nef protein and with selected Gag peptides that showed response by elispot (see methods). Of note, we excluded peptides 41, 42, and 61 to avoid stimulation of infected cells of interest (Figure 5B). In parallel, CD8-depleted PBMCs were stimulated with either peptide 42 or 61 for 24 hours; peptides were then removed, and cells were plated with stimulated CD8$^+$ T cells at a 1:3 effector-to-target ratio and cultured for

10 days. Virus production, monitored from day 3 to day 10, was markedly reduced by $CD8^+$ T cells; however, Chr7.d11sc was significantly more impacted than ZNF721i (1467- vs 3.7-fold reduction in HIV-1 RNA copies/mL at day 10, p=0.02, Figure 5C-E). Although $CD8^+$ T cells had a lesser effect on cell proliferation, likely reflecting that most infected cells divide without the expression of viral antigens (13, 48), cells carrying Chr7.d11sc proliferated significantly less than the ZNF721i clone (Figure 5F, G and I). Of note, cells harboring the ZNF470i provirus were not affected by $CD8^+$ T cells (Figure 5H), indicating that in this context CTLs specifically recognized and killed only peptide-stimulated infected cells, rather than via non-specific effector molecule production and non-cytolytic effects (49-51). In the presence of activated $CD8^+$ T cells, cells harboring Chr7.d11sc decreased to about 40% of the cells in the control arm, while the ZNF721i provirus was barely affected (95% of cells without CD8s, p=0.03; Figure 5I). Coculture with $CD8^+$ T cells had a strikingly distinct effect on virus production and cell proliferation, suggesting that only virus producing cells were eliminated. Moreover, the amount of virus produced on a per cell level may affect the efficiency of immune recognition and the HIV RNA levels at the end of culture. Indeed, in our experiments we observed that the estimated inducibility of Chr7.d11sc was significantly reduced by $CD8^+$ T cells (average RNA/DNA 169 versus 0.24, p=0.002, Figure 5J), while ZNF721i was only modestly affected (0.27 versus 0.08, p=ns). Together, these results demonstrate that the lower inducibility of the ZNF721i provirus allowed escape from CTL recognition by proliferating upon T cell activation with negligible expression of viral antigens, which can explain its marked clonal expansion observed in vivo after CRT and immunotherapy.

Discussion

The activation of latently infected $CD4^+$ T cells with potent mitogens results in viral transcription and the reversal of latency in many clones (52). However, this process is stochastic and there is mounting evidence that following activation, some infected T cell clones can proliferate without producing virus (13, 14, 48). This process has major implications for the persistence of infected $CD4^+$ T cell clones in the presence of HIV-1-specific $CD8^+$ T cells (53-55).

In this case report we characterized clonal dynamics before, during, and after chemoradiation and immunotherapy in an EC with metastatic lung cancer. The contraction of individual clones is remarkable as chemotherapy and immunotherapy generally did not affect the size of the latent reservoir in prior studies (26, 56, 57). The same pattern of a modest but transient reduction in intact proviral DNA was recently described in kidney transplant patients receiving induction immunosuppression (33). Our results extend these findings by tracking individual clones with integration site analysis. Three clones in this study are especially interesting. The large clone which contains replication-competent ZNF470i provirus was stable during treatment. In contrast the cells carrying the ZNF721i provirus, which recognizes the Gag peptide STLQEQIGWMTNNPP (241-255), underwent a 70-fold expansion after chemotherapy was completed. This may explain why there was only a modest decline in intact proviral DNA despite the marked reduction in the number of total clones after chemoradiation. The third clone, Chr7.d11sc, contains a nearly intact provirus and recognizes the overlapping Gag peptides EKAFSPEVIPMFSAL (162-176) and SPEVIPMFSALSEGA (166-180). To the best of our knowledge, this is the first study to identify the exact epitope recognized by infected T cell clones. This is important as epitope identification could enable the specific activation of latently infected T cells as part of HIV-1 cure strategies. While the peptides triggered both viral transcription and proliferation of both the ZNF721i and Chr7.d11sc clones, the degree of viral transcription was significantly lower for the ZNF721i provirus. This difference in viral transcription between the two clones was associated with

differences in the ability of autologous CD8+ T cells to inhibit clonal expansion. While the presence of CD8+ T cells resulted in a 60% inhibition of proliferation of cells with the Chr7.d11sc provirus, CD8+ T cells had no effect on the proliferation of the clone carrying ZNF721i. This difference is particularly interesting given the fact that the Chr7.d11sc provirus has accumulated several escape mutations while the ZNF721i provirus has no escape mutations in Gag and Nef epitopes. The presence of escape mutations in Chr7.d11sc suggests that some of the reservoir cells in ES24 have been subjected to $CD8^+$ T cell selective pressure in vivo. While these mutations are rare in proviruses from EC, they have been described and virologic control may be maintained by de novo CD8+ T cell responses that can inhibit replication of autologous escape mutants (58-61).

The 60% reduction of the Chr7.11sc provirus may underestimate of the ability of $CD8^+$ T cells to inhibit the expansion of virus producing cells given the stochastic nature of latency reversal. In a prior study that subjected $CD4^+$ T cells to multiple rounds of potent activation, a mean of just 60% of the infected cells that eventually produced virus did so after the first round of activation (36). Thus, it is likely that only a subset of cells of the Chr7.d11sc provirus produced virus in response to 24 hours of stimulation with cognate peptide. The 3-log reduction in Chr7.d11sc RNA in the presence of $CD8^+$ T cells suggests that most of the cells that produced virus were eliminated, and the remaining cells were not targeted because they did not express viral proteins. The ZNF721i provirus is significantly less inducible than the Chr7.d11sc provirus which may contribute to immune evasion and explain the rapid expansion of cells with the ZNF721i provirus in contrast to the Chr7.d11sc provirus which is present at a much lower frequency in vivo.

Our study is limited by the fact that it involves a single patient who is an elite controller. Even though this case may not be representative of most people without spontaneous HIV-1 control, a progressive enrichment of intact proviruses in ZNF genes has been observed in people living with HIV-1 on long-term ART. It is also possible that the process of clonal expansion was affected by

his malignancy. However, we describe the effects of chemoradiation and immunotherapy on individual clones and study the effects of T cell activation on infected clones using a physiologic system with individual cognate peptides. In addition, our findings can be extended to larger cohorts of ECs, whose HIV-1-reactive $CD4^+$ clones can be easily detected (62). The highly dominant ZNF721i provirus in Gag-reactive $CD4^+$ clones, found in this participant, has not been described before. However, the presence of HIV-1-reactive clones, albeit rarer among all infected cells, is generalizable to both EC and normal progressors on long-term ART (20, 40, 63). Our findings suggest that the selective recognition and elimination of transcriptionally active proviruses like Chr7.d11sc by the immune system could explain the predominance of clonally expanded proviruses integrated into transcriptionally repressed sites in HIV-1 controllers and people on long-term ART (18). The experimental evidence provided here further supports recent reports of genotypic and phenotypic signatures of intact proviruses, results of a dynamic proviral landscape shaped over time by the immune system (64).

However, additional work is needed to understand whether specific host and proviral factors contribute to the establishment and maintenance the so called “deeper latency” of some intact proviruses in ZNF genes. Whether rare proviruses are merely caught in between the evolutionary arms race against transposable elements, or specifically targeted by repressive epigenetic mediators is yet to be determined (65, 66). Moreover, our data also suggest that strategies that use agents like IL-15 which induce proliferation to augment effector responses may paradoxically increase the size of the reservoir by causing expansion in the absence of virus expression of proviruses like ZNF721i that can partially evade the immune system (67). Finally, it should be noted that viral particle production does occur even from proviruses like ZNF721i, and thus immune recognition and elimination of productively infected cells would still be essential for elite control and for preventing viral rebound in most people on ART.

353

Methods

Human Subjects. The study participant, a 66-year-old Afro-American male, has been anonymized as ES24. He has been diagnosed HIV-1-positive in 2009. Seven total longitudinal time points have been collected for this study. The participant's PBMCs were obtained from whole blood by Ficoll-based density separation, and $CD4^+$ T cells were isolated by magnetic bead-based negative selection (Miltenyi) Activated lymphoblasts and irradiated-PBMCs from HIV-1-negative individuals were used in the QVOA assay.

Intact Proviral DNA Assay (IPDA). The IPDA was performed as previously described (68) on $CD4^+$ T cells, using the QX200 Droplet Digital PCR System (Bio-Rad). The assay interrogates two specific regions of the HIV-1 genome to genetically discriminate between defective and intact proviral DNA.

Quantitative Viral Outgrowth Assay (QVOA). The QVOA was performed as previously described (58, 69) from isolated $CD4^+$ T cells. Following identification of p24+ wells, supernatants were collected and extracted to sequence the virion-associated HIV-1 RNA in either the *nef* or U5-*gag* region. (15).

Integration site analysis. Integration site analysis was performed with two different approaches. Linker-mediated PCR was performed on genomic DNA from bulk CD4+ T cells following controlled sonication, as previously described (70). PCR products obtained were purified, pooled, and sequenced on an Illumina MiSeq. Integration sites were determined from the sequence data using the INSPIIRED pipeline (https://github.com/BushmanLab/). Conversely, the Lenti-X Integration Site Analysis Kit (Clontech) was used to characterize the integration sites from limiting diluted gDNA subjected to whole genome amplification (WGA), using the Advance Single Cell Repli-G Kit (Qiagen), as previously described (35). PCR products obtained with this approach were sequenced by Sanger Sequencing (Azenta).

Provirus sequencing. Genomic DNA (gDNA) was isolated accordingly to the number of cells. For samples lower than one million cells, DNA was extracted following Wiegand *et al.* (46), otherwise the QIAamp DNA Mini Kit (QIAGEN) was used. Following limiting dilution, proviral sequences of ZNF470i and ZNF721i were recovered by FLIPS (71) and MIPseq (35), respectively. Due to the limited presence of Chr7.d11sc, its viral sequence was recovered from virion-associated HIV-1 RNA in the supernatant, obtained from CD8-depleted PBMC stimulation experiment (see below). If primers commonly used for full-length proviral sequencing failed due to mismatches, specific primers were designed. Finally, to reconstruct the full proviral sequence, primers annealing in the human genome flanking the integration site were used to recover the LTR regions. All the primers used in this study are detailed in Supplemental Table S2.

Total LTR copies. To quantify all LTR copies we used primers and probe targeting the R-U5 junction, as previously described (38, 72). In brief, gDNA from total $CD4^+$ T cells undergoes controlled physical shearing so that the LTRs from the same provirus are not in linkage and are captured in separate partitions. The primers and probe anneal to the R-U5 junction, so that both LTRs are quantified regardless of 5' or 3' end. Digital PCR reactions were run using the Qiacuity One Digital PCR System (Qiagen) with an initial denaturation step of 95 °C for 2', followed by 45 cycles each including 95 °C for 15'' and 58°C for 30''. This assay can be run in a multiplex reaction with the integration site PCR described below. Oligo sequences are described in Supplemental Table S2.

Quantification of proviruses of interest by digital PCR. Specific assays to quantify ZNF470i and ZNF721i were designed on the host-U3 junction, with the fluorescently labelled probe annealing across the site of HIV-integration, as previously described (20). In addition, exploiting the 11-nt deletion present in the primer binding site of Chr7.d11sc (HXB2 position 660-670), we designed an assay based on competition probes to discriminate the Chr7.d11sc virus from other variants. To confirm that the virus produced upon stimulation with peptide 61 was indeed from

ZNF721i provirus, we performed SGS from the supernatant (Supplemental Figure S5). Copies of targets of interests were normalized based on cell genome equivalents screened, calculated by RPP30, as previously described (68). Primers and probes are detailed in Supplemental Table S2. Digital PCR reactions were run using the Qiacuity One Digital PCR System (Qiagen) with an initial denaturation step of 95 °C for 2', followed by 45 cycles each including 95 °C for 15'' and 58°C for 30''.

Clonal expansion assay. PBMCs were obtained from blood via a standard Ficoll procedure. The cells were subjected to two rounds of $CD8^+$ T cell depletion using negative selection beads (Miltenyi). CD8-depleted PBMCs were then cultured in RPMI (Gibco) with 10% fetal calf serum (Gibco) and 10 units/ml of IL2 at a concentration of 1 million cells per ml. The antiretroviral drugs raltegravir and efavirenz were obtained from NIH HIV Reagent Program. Four million cells were cultured in each well of a 12-well plate and stimulated with overlapping Gag peptides from NIH AIDS Reagent Program at a concentration of 10 ug/ml. To identify the individual Gag peptides that induced clonal expansion, CD8-depleted PBMCs were stimulated with 11 different pools containing 10-13 peptides each. Each individual peptide from the 2 pools that resulted in virus production was then tested individually at a concentration of 10 µg/ml.

RNA extraction and cDNA synthesis. Culture supernatants were spun at 3500g for 15' at 4 °C and transferred to clean tubes for an additional step of centrifugation at 21000g for 2h at 4 °C. Viral pellets underwent RNA extraction, as previously descried (73). RNA was immediately used for reverse transcription using Super Script III with a participant-specific primer located in *gag*. cDNA synthesis reaction was at 55°C for 50', followed by an inactivation step at 85 °C for 5'. cDNA was quantified by a dPCR assay targeting the U5-PBS region, or used for single genome sequencing, as described above. To quantify and sequence cell-associated RNA from peripheral blood $CD4^+$ T cells, we isolated total RNA and gDNA from small aliquots of cells (700,000) as

previously described (46). HIV-1 RNA U5-PBS RNA were quantified as described above, and normalized to million cell equivalents by RPP30 copies from gDNA.

TCR sequencing and quantification of VDJ rearrangements of interest. Genomic DNA from cultured cells was subjected to TCRβ sequencing, as previously described (74). To measure CASSLTGGGEQFF, we designed a digital PCR assay with primers flanking the VDJ rearrangement of the TCR beta chain, as previously described (20). To increase specificity and avoid a polymeric region of guanosines, we designed two different probes annealing across the VD and DJ junctions, fluorescently labelled with FAM and HEX, respectively. Only double positive partitions were used to quantify the clonotype of interest (Supplemental Figure S4 and Supplemental Table S2). To confirm that the CASSLTGGGEQFF CDR3 belonged to the cells carrying ZNF721i, we distributed 800 CD8-depleted PBMCs over 96-well plates. After whole genome amplification, we identified wells positive for any provirus, ZNF721i, and CASSLTGGGEQFF by digital PCR. We used combinatorial statistics to calculate the probability that ZNF721i and CASSLTGGGEQFF would co-localize in the same wells by chance, as previously described (20) (see Supplemental Figure S4).

Intracellular cytokine assay. One million PBMCs were cultured in each well of a round bottom 96 well plate overnight in 200ul of RPMI with 10% fetal calf serum with 2ug/ml of antibodies to CD28 and CD49d (BD Biosciences) in the presence of 1ul/ml of Golgi Plug and Golgi Stop (BD Biosciences). The cells were then washed and stained with live/dead stain (Zombie NIR, BioLegend) and antibodies to CD3, CD4 and CD8 (Pacific Blue, UCHT1, 558117; PerCP/Cyanine5.5, RPA-T4, 300530 and Brilliant Violet 605, RPA-T8, 301040, respectively). The cells were then fixed and permeabilized with BD Cytofix/Cytoperm (BD Biosciences) and stained with antibodies to IFN-g, TNF-a, and IL2 (APC, B27, 506510; PE-Cy7, Mab11, 557647 and PE, MQ1-17H12, 500307, respectively). The cells were then read on a BD LSR Fortessa (BD Biosciences). Data were analyzed using FlowJo 10.0.8 software (FlowJo, LLC).

CD8$^+$ T cell Assay. To induce potent cytotoxic function, CD8$^+$ T cells were first stimulated with peptides for 7 days (75, 76). On day -7, PBMCs were stimulated with overlapping Nef peptides covering the entire protein and 10 Gag peptides he had previously responded to including Gag 24-39 (GKKKYKLKHIVWASR), Gag 93-107 (EVKDTKEALEKIEEE), Gag 141-155 (QMVHQAISPRTLNAW), Gag 269-283 (GLNKIVRMYSPTSIL), Gag 297-311 (VDRFYKTLRAEQASQ), Gag 333-347 (ILKALGPAATLEEMM), Gag 365-379 (EAMSQVTNSATIMMQ), Gag 433-447 (FLGKIWPSHKGRPGN), Gag 453-467 (PEPTAPPEESFRFGE), Gag 483-497 (KELYPLASLRSLFGN) in R10 media with 10 units/mL of IL2, efavirenz, and raltegravir. Gag peptides 41, 42, and 61 were all excluded so as not to activate and expand T cells specific for these peptides which could kill target cells that had residual peptides present on MHC molecules after activation. On day -1, fresh PBMCs were subjected to two rounds of CD8+ T cell depletion with Miltenyi micro beads. The cells were then stimulated for 24 hours with peptide 41 and 61 at a concentration of 10 ug/ml in R10 media with 10 units/mL of IL2 with efavirenz and raltegravir. On day 0, the CD8 depleted PBMCs were washed to remove peptide and plated at 3 million cells per well in a 24 well plate with 3 replicates per condition. CD8$^+$ T cells were isolated from the PBMCs that had been stimulated with peptides at day -7 using Miltenyi micro beads. A million CD8$^+$ T cells were added to 3 million stimulated CD8-depleted PBMCs. Half of the media was removed and fresh R10 with 10 units/ml of IL2 was added on days 3 and 7, and efavirenz and raltegravir was added on day 7. On day 10, CD4$^+$ T cells were isolated by negative selection (Stem Cell) in 96 well plates. Genomic DNA was extracted from about 0.5 million CD4$^+$ T cells and used for downstream dPCR assays.

Visualization of CHIP-seq data. Data from primary CD4+ T cells were obtained from the ROADMAP Epigenomics program database (dataset IDs E037, E038, E039, E040, E041, E042, E043); chromatin states were visualized via Epigenome Browser (77) and Epilogos (https://epilogos.altius.org/) (45).

Quantification and statistical analysis. Descriptive statistics, tests for normality, 2-tailed Student's t-test and one-way ANOVA tests were used to determine statistical significance using GraphPad Prism v8.0. Chi square and Fisher exact test were calculated in Excel. Combinatorial statistics for provirus and TCR co-occurrence were calculated as previously described (20, 78). A P value less than 0.05 was considered significant, unless otherwise stated.

Data and code availability. Single genome sequences and full-length proviral genome sequences retrieved for this work have been deposited to GenBank (accession numbers OR496614-OR496825 and pending), and OR496826-OR496828) and the NCI provirus database. Integration site data are available at the NCBI Bioproject Sequence Read Archive (reference PRNJA988676) and the NCI retrovirus integration database (https://rid.ncifcrf.gov/). TCRβ sequencing data are available at the NCBI Gene expression omnibus (GSM7577878-GSM7577889). Supporting data values used for Figures 1 to 5 and all Supplemental Figures are available in a separate excel file. All datasets generated from this study are available from the lead contact upon request, except the private health information of the study participant. This paper does not report original code.

Study Approval. The Johns Hopkins Institutional Review Board approved this study. The study participant provided written, informed consent before enrollment.

Authors Contributions

FRS, and JNB conceived the study. AKK, FD, CCG, BAW, AAC, RTV and KR performed experiments and analyzed data. JNB, AMR, and EPS enrolled the study participant, gathered their clinical history and samples. HR and FDB conducted integration site experiments and analysis. KNS performed TCR sequencing and analysis. FRS, FD, RTV and JNB conducted analyses and generated figures. FRS and JNB wrote the manuscript and received feedback and final approval from all authors.

Acknowledgements

We deeply thank the study participant for his commitment in volunteering in this study. We thank Aoife Roche and John Everett for the useful discussions leading to this work. FRS is supported by the Office of the NIH Director and National Institute of Dental & Craniofacial Research (DP5OD031834), the Johns Hopkins University CFAR (P30AI094189) and the NIAID (PAVE, UM1AI164566). JB is supported by the NIH grant R01AI140789 and R21AI172542. HR and FDB were supported by R01AI129661, U19AI117950, U19AI149680, UM1AI164570, R01CA241762, The PennCHOP Microbiome Program, The Center for AIDS Research at the University of Pennsylvania (P30-AI045008)

References

1. Whitney JB, Hill AL, Sanisetty S, Penaloza-MacMaster P, Liu J, Shetty M, et al. Rapid seeding of the viral reservoir prior to SIV viraemia in rhesus monkeys. *Nature.* 2014;512(7512):74-7.
2. Colby DJ, Trautmann L, Pinyakorn S, Leyre L, Pagliuzza A, Kroon E, et al. Rapid HIV RNA rebound after antiretroviral treatment interruption in persons durably suppressed in Fiebig I acute HIV infection. *Nat Med.* 2018;24(7):923-6.
3. Chun TW, Finzi D, Margolick J, Chadwick K, Schwartz D, and Siliciano RF. In vivo fate of HIV-1-infected T cells: quantitative analysis of the transition to stable latency. *Nat Med.* 1995;1(12):1284-90.
4. Finzi D, Hermankova M, Pierson T, Carruth LM, Buck C, Chaisson RE, et al. Identification of a reservoir for HIV-1 in patients on highly active antiretroviral therapy. *Science.* 1997;278(5341):1295-300.
5. Siliciano JD, Kajdas J, Finzi D, Quinn TC, Chadwick K, Margolick JB, et al. Long-term follow-up studies confirm the stability of the latent reservoir for HIV-1 in resting CD4+ T cells. *Nat Med.* 2003;9(6):727-8.
6. Crooks AM, Bateson R, Cope AB, Dahl NP, Griggs MK, Kuruc JD, et al. Precise Quantitation of the Latent HIV-1 Reservoir: Implications for Eradication Strategies. *J Infect Dis.* 2015;212(9):1361-5.
7. Deeks SG, and Walker BD. Human immunodeficiency virus controllers: mechanisms of durable virus control in the absence of antiretroviral therapy. *Immunity.* 2007;27(3):406-16.
8. Migueles SA, and Connors M. Success and failure of the cellular immune response against HIV-1. *Nat Immunol.* 2015;16(6):563-70.
9. Saez-Cirion A, Pancino G, Sinet M, Venet A, Lambotte O, and group AEHCs. HIV controllers: how do they tame the virus? *Trends Immunol.* 2007;28(12):532-40.
10. Li JZ, and Blankson JN. How elite controllers and posttreatment controllers inform our search for an HIV-1 cure. *J Clin Invest.* 2021;131(11).
11. Kennedy BD, Blazkova J, Justement JS, Shi V, Rai MA, Manning MR, et al. Comprehensive analysis of HIV reservoirs in elite controllers. *J Clin Invest.* 2023;133(3).
12. Boritz EA, Darko S, Swaszek L, Wolf G, Wells D, Wu X, et al. Multiple Origins of Virus Persistence during Natural Control of HIV Infection. *Cell.* 2016;166(4):1004-15.
13. Hosmane NN, Kwon KJ, Bruner KM, Capoferri AA, Beg S, Rosenbloom DI, et al. Proliferation of latently infected CD4(+) T cells carrying replication-competent HIV-1: Potential role in latent reservoir dynamics. *J Exp Med.* 2017;214(4):959-72.
14. Bui JK, Sobolewski MD, Keele BF, Spindler J, Musick A, Wiegand A, et al. Proviruses with identical sequences comprise a large fraction of the replication-competent HIV reservoir. *PLOS Pathogens.* 2017;13(3):e1006283.
15. Veenhuis RT, Kwaa AK, Garliss CC, Latanich R, Salgado M, Pohlmeyer CW, et al. Long-term remission despite clonal expansion of replication-competent HIV-1 isolates. *JCI Insight.* 2018;3(18).
16. Coffin JM, Wells DW, Zerbato JM, Kuruc JD, Guo S, Luke BT, et al. Clones of infected cells arise early in HIV-infected individuals. *JCI Insight.* 2019;4(12).
17. Cohn LB, Chomont N, and Deeks SG. The Biology of the HIV-1 Latent Reservoir and Implications for Cure Strategies. *Cell Host Microbe.* 2020;27(4):519-30.
18. Jiang C, Lian X, Gao C, Sun X, Einkauf KB, Chevalier JM, et al. Distinct viral reservoirs in individuals with spontaneous control of HIV-1. *Nature.* 2020;585(7824):261-7.

19. Pinzone MR, Weissman S, Pasternak AO, Zurakowski R, Migueles S, and O'Doherty U. Naive infection predicts reservoir diversity and is a formidable hurdle to HIV eradication. *JCI Insight.* 2021;6(16).
20. Simonetti FR, Zhang H, Soroosh GP, Duan J, Rhodehouse K, Hill AL, et al. Antigen-driven clonal selection shapes the persistence of HIV-1-infected CD4+ T cells in vivo. *J Clin Invest.* 2021;131(3).
21. Guo S, Luke BT, Henry AR, Darko S, Brandt LD, Su L, et al. HIV infected CD4+ T cell clones are more stable than uninfected clones during long-term antiretroviral therapy. *PLoS Pathog.* 2022;18(8):e1010726.
22. Bushman FD. Retroviral Insertional Mutagenesis in Humans: Evidence for Four Genetic Mechanisms Promoting Expansion of Cell Clones. *Mol Ther.* 2020;28(2):352-6.
23. Coffin JM, Bale MJ, Wells D, Guo S, Luke B, Zerbato JM, et al. Integration in oncogenes plays only a minor role in determining the in vivo distribution of HIV integration sites before or during suppressive antiretroviral therapy. *PLoS Pathog.* 2021;17(4):e1009141.
24. Deeks SG, Archin N, Cannon P, Collins S, Jones RB, de Jong M, et al. Research priorities for an HIV cure: International AIDS Society Global Scientific Strategy 2021. *Nat Med.* 2021;27(12):2085-98.
25. Schiffer JT, Levy C, Hughes SM, Pandey U, Padullo M, Jerome KR, et al. Stable HIV Reservoir Despite Prolonged Low-Dose Mycophenolate to Limit CD4+ T-cell Proliferation. *Open Forum Infect Dis.* 2022;9(12):ofac620.
26. Cillo AR, Krishnan S, McMahon DK, Mitsuyasu RT, Para MF, and Mellors JW. Impact of chemotherapy for HIV-1 related lymphoma on residual viremia and cellular HIV-1 DNA in patients on suppressive antiretroviral therapy. *PLoS One.* 2014;9(3):e92118.
27. Lian X, Gao C, Sun X, Jiang C, Einkauf KB, Seiger KW, et al. Signatures of immune selection in intact and defective proviruses distinguish HIV-1 elite controllers. *Sci Transl Med.* 2021;13(624):eabl4097.
28. Lian X, Seiger KW, Parsons EM, Gao C, Sun W, Gladkov GT, et al. Progressive transformation of the HIV-1 reservoir cell profile over two decades of antiviral therapy. *Cell Host Microbe.* 2023;31(1):83-96 e5.
29. Huang AS, Ramos V, Oliveira TY, Gaebler C, Jankovic M, Nussenzweig MC, et al. Integration features of intact latent HIV-1 in CD4+ T cell clones contribute to viral persistence. *J Exp Med.* 2021;218(12).
30. Einkauf KB, Osborn MR, Gao C, Sun W, Sun X, Lian X, et al. Parallel analysis of transcription, integration, and sequence of single HIV-1 proviruses. *Cell.* 2022;185(2):266-82 e15.
31. Halvas EK, Joseph KW, Brandt LD, Guo S, Sobolewski MD, Jacobs JL, et al. HIV-1 viremia not suppressible by antiretroviral therapy can originate from large T cell clones producing infectious virus. *J Clin Invest.* 2020;130(11):5847-57.
32. Zhang C, Palashati H, Tan Q, Ku W, Miao Y, Xiong H, et al. Immediate and substantial evolution of T-cell repertoire in peripheral blood and tumor microenvironment of patients with esophageal squamous cell carcinoma treated with preoperative chemotherapy. *Carcinogenesis.* 2018;39(11):1389-98.
33. Benner SE, Eby Y, Zhu X, Fernandez RE, Patel EU, Ruff JE, et al. The effect of induction immunosuppression for kidney transplant on the latent HIV reservoir. *JCI Insight.* 2022;7(21).
34. Han Y, Lassen K, Monie D, Sedaghat AR, Shimoji S, Liu X, et al. Resting CD4+ T cells from human immunodeficiency virus type 1 (HIV-1)-infected individuals carry integrated HIV-1 genomes within actively transcribed host genes. *J Virol.* 2004;78(12):6122-33.
35. Einkauf KB, Lee GQ, Gao C, Sharaf R, Sun X, Hua S, et al. Intact HIV-1 proviruses accumulate at distinct chromosomal positions during prolonged antiretroviral therapy. *J Clin Invest.* 2019;129(3):988-98.

36. Lukic S, Nicolas JC, and Levine AJ. The diversity of zinc-finger genes on human chromosome 19 provides an evolutionary mechanism for defense against inherited endogenous retroviruses. *Cell Death Differ.* 2014;21(3):381-7.
37. Brandt LD, Guo S, Joseph KW, Jacobs JL, Naqvi A, Coffin JM, et al. Tracking HIV-1-Infected Cell Clones Using Integration Site-Specific qPCR. *Viruses.* 2021;13(7).
38. White JA, Wu F, Yasin S, Moskovljevic M, Varriale J, Dragoni F, et al. Clonally expanded HIV-1 proviruses with 5'-Leader defects can give rise to nonsuppressible residual viremia. *J Clin Invest.* 2023.
39. Simonetti FR, White JA, Tumiotto C, Ritter KD, Cai M, Gandhi RT, et al. Intact proviral DNA assay analysis of large cohorts of people with HIV provides a benchmark for the frequency and composition of persistent proviral DNA. *Proc Natl Acad Sci U S A.* 2020;117(31):18692-700.
40. Mendoza P, Jackson JR, Oliveira TY, Gaebler C, Ramos V, Caskey M, et al. Antigen-responsive CD4+ T cell clones contribute to the HIV-1 latent reservoir. *J Exp Med.* 2020;217(7).
41. Collora JA, Liu R, Pinto-Santini D, Ravindra N, Ganoza C, Lama JR, et al. Single-cell multiomics reveals persistence of HIV-1 in expanded cytotoxic T cell clones. *Immunity.* 2022;55(6):1013-31 e7.
42. Gantner P, Pagliuzza A, Pardons M, Ramgopal M, Routy JP, Fromentin R, et al. Single-cell TCR sequencing reveals phenotypically diverse clonally expanded cells harboring inducible HIV proviruses during ART. *Nat Commun.* 2020;11(1):4089.
43. Cole B, Lambrechts L, Gantner P, Noppe Y, Bonine N, Witkowski W, et al. In-depth single-cell analysis of translation-competent HIV-1 reservoirs identifies cellular sources of plasma viremia. *Nat Commun.* 2021;12(1):3727.
44. Sleiman D, Goldschmidt V, Barraud P, Marquet R, Paillart JC, and Tisne C. Initiation of HIV-1 reverse transcription and functional role of nucleocapsid-mediated tRNA/viral genome interactions. *Virus Res.* 2012;169(2):324-39.
45. Roadmap Epigenomics C, Kundaje A, Meuleman W, Ernst J, Bilenky M, Yen A, et al. Integrative analysis of 111 reference human epigenomes. *Nature.* 2015;518(7539):317-30.
46. Wiegand A, Spindler J, Hong FF, Shao W, Cyktor JC, Cillo AR, et al. Single-cell analysis of HIV-1 transcriptional activity reveals expression of proviruses in expanded clones during ART. *Proc Natl Acad Sci U S A.* 2017;114(18):E3659-E68.
47. Goulder PJ, Bunce M, Krausa P, McIntyre K, Crowley S, Morgan B, et al. Novel, cross-restricted, conserved, and immunodominant cytotoxic T lymphocyte epitopes in slow progressors in HIV type 1 infection. *AIDS Res Hum Retroviruses.* 1996;12(18):1691-8.
48. Musick A, Spindler J, Boritz E, Perez L, Crespo-Velez D, Patro SC, et al. HIV Infected T Cells Can Proliferate in vivo Without Inducing Expression of the Integrated Provirus. *Front Microbiol.* 2019;10:2204.
49. Cocchi F, DeVico AL, Garzino-Demo A, Arya SK, Gallo RC, and Lusso P. Identification of RANTES, MIP-1 alpha, and MIP-1 beta as the major HIV-suppressive factors produced by CD8+ T cells. *Science.* 1995;270(5243):1811-5.
50. Mackewicz CE, Blackbourn DJ, and Levy JA. CD8+ T cells suppress human immunodeficiency virus replication by inhibiting viral transcription. *Proc Natl Acad Sci U S A.* 1995;92(6):2308-12.
51. Zanoni M, Palesch D, Pinacchio C, Statzu M, Tharp GK, Paiardini M, et al. Innate, non-cytolytic CD8+ T cell-mediated suppression of HIV replication by MHC-independent inhibition of virus transcription. *PLoS Pathog.* 2020;16(9):e1008821.
52. Sengupta S, and Siliciano RF. Targeting the Latent Reservoir for HIV-1. *Immunity.* 2018;48(5):872-95.

53. Shan L, Deng K, Shroff NS, Durand CM, Rabi SA, Yang HC, et al. Stimulation of HIV-1-specific cytolytic T lymphocytes facilitates elimination of latent viral reservoir after virus reactivation. *Immunity.* 2012;36(3):491-501.
54. Jones RB, and Walker BD. HIV-specific CD8(+) T cells and HIV eradication. *J Clin Invest.* 2016;126(2):455-63.
55. Warren JA, Zhou S, Xu Y, Moeser MJ, MacMillan DR, Council O, et al. The HIV-1 latent reservoir is largely sensitive to circulating T cells. *Elife.* 2020;9.
56. Rasmussen TA, Rajdev L, Rhodes A, Dantanarayana A, Tennakoon S, Chea S, et al. Impact of Anti-PD-1 and Anti-CTLA-4 on the Human Immunodeficiency Virus (HIV) Reservoir in People Living With HIV With Cancer on Antiretroviral Therapy: The AIDS Malignancy Consortium 095 Study. *Clin Infect Dis.* 2021;73(7):e1973-e81.
57. Uldrick TS, Adams SV, Fromentin R, Roche M, Fling SP, Goncalves PH, et al. Pembrolizumab induces HIV latency reversal in people living with HIV and cancer on antiretroviral therapy. *Sci Transl Med.* 2022;14(629):eabl3836.
58. Bailey JR, Williams TM, Siliciano RF, and Blankson JN. Maintenance of viral suppression in HIV-1-infected HLA-B*57+ elite suppressors despite CTL escape mutations. *J Exp Med.* 2006;203(5):1357-69.
59. Miura T, Brumme CJ, Brockman MA, Brumme ZL, Pereyra F, Block BL, et al. HLA-associated viral mutations are common in human immunodeficiency virus type 1 elite controllers. *J Virol.* 2009;83(7):3407-12.
60. O'Connell KA, Hegarty RW, Siliciano RF, and Blankson JN. Viral suppression of multiple escape mutants by de novo CD8(+) T cell responses in a human immunodeficiency virus-1 infected elite suppressor. *Retrovirology.* 2011;8:63.
61. Pohlmeyer CW, Buckheit RW, 3rd, Siliciano RF, and Blankson JN. CD8+ T cells from HLA-B*57 elite suppressors effectively suppress replication of HIV-1 escape mutants. *Retrovirology.* 2013;10:152.
62. Morou A, Brunet-Ratnasingham E, Dube M, Charlebois R, Mercier E, Darko S, et al. Altered differentiation is central to HIV-specific CD4(+) T cell dysfunction in progressive disease. *Nat Immunol.* 2019;20(8):1059-70.
63. Mann JFS, Pankrac J, Klein K, McKay PF, King DFL, Gibson R, et al. A targeted reactivation of latent HIV-1 using an activator vector in patient samples from acute infection. *EBioMedicine.* 2020;59:102853.
64. Sun W, Gao C, Hartana CA, Osborn MR, Einkauf KB, Lian X, et al. Phenotypic signatures of immune selection in HIV-1 reservoir cells. *Nature.* 2023;614(7947):309-17.
65. Bruno M, Mahgoub M, and Macfarlan TS. The Arms Race Between KRAB-Zinc Finger Proteins and Endogenous Retroelements and Its Impact on Mammals. *Annu Rev Genet.* 2019;53:393-416.
66. Seczynska M, and Lehner PJ. The sound of silence: mechanisms and implications of HUSH complex function. *Trends Genet.* 2023;39(4):251-67.
67. Li Y, Gao H, Clark KM, and Shan L. IL15 enhances HIV-1 infection by promoting survival and proliferation of CCR5+CD4+ T cells. *JCI Insight.* 2023.
68. Bruner KM, Wang Z, Simonetti FR, Bender AM, Kwon KJ, Sengupta S, et al. A quantitative approach for measuring the reservoir of latent HIV-1 proviruses. *Nature.* 2019;566(7742):120-5.
69. Laird GM, Eisele EE, Rabi SA, Lai J, Chioma S, Blankson JN, et al. Rapid Quantification of the Latent Reservoir for HIV-1 Using a Viral Outgrowth Assay. *PLOS Pathogens.* 2013;9(5):e1003398.
70. Sherman E, Nobles C, Berry CC, Six E, Wu Y, Dryga A, et al. INSPIIRED: A Pipeline for Quantitative Analysis of Sites of New DNA Integration in Cellular Genomes. *Mol Ther Methods Clin Dev.* 2017;4:39-49.

71. Hiener B, Horsburgh BA, Eden JS, Barton K, Schlub TE, Lee E, et al. Identification of Genetically Intact HIV-1 Proviruses in Specific CD4(+) T Cells from Effectively Treated Participants. *Cell Rep.* 2017;21(3):813-22.
72. Anderson EM, Simonetti FR, Gorelick RJ, Hill S, Gouzoulis MA, Bell J, et al. Dynamic Shifts in the HIV Proviral Landscape During Long Term Combination Antiretroviral Therapy: Implications for Persistence and Control of HIV Infections. *Viruses.* 2020;12(2).
73. Tosiano MA, Jacobs JL, Shutt KA, Cyktor JC, and Mellors JW. A Simpler and More Sensitive Single-Copy HIV-1 RNA Assay for Quantification of Persistent HIV-1 Viremia in Individuals on Suppressive Antiretroviral Therapy. *J Clin Microbiol.* 2019;57(3).
74. Chan HY, Zhang J, Garliss CC, Kwaa AK, Blankson JN, and Smith KN. A T Cell Receptor Sequencing-Based Assay Identifies Cross-Reactive Recall CD8(+) T Cell Clonotypes Against Autologous HIV-1 Epitope Variants. *Front Immunol.* 2020;11:591.
75. Migueles SA, Osborne CM, Royce C, Compton AA, Joshi RP, Weeks KA, et al. Lytic granule loading of CD8+ T cells is required for HIV-infected cell elimination associated with immune control. *Immunity.* 2008;29(6):1009-21.
76. Migueles SA, Rogan DC, Gavil NV, Kelly EP, Toulmin SA, Wang LT, et al. Antigenic Restimulation of Virus-Specific Memory CD8(+) T Cells Requires Days of Lytic Protein Accumulation for Maximal Cytotoxic Capacity. *J Virol.* 2020;94(23).
77. Li D, Purushotham D, Harrison JK, Hsu S, Zhuo X, Fan C, et al. WashU Epigenome Browser update 2022. *Nucleic Acids Res.* 2022;50(W1):W774-W81.
78. Howie B, Sherwood AM, Berkebile AD, Berka J, Emerson RO, Williamson DW, et al. High-throughput pairing of T cell receptor alpha and beta sequences. *Sci Transl Med.* 2015;7(301):301ra131.

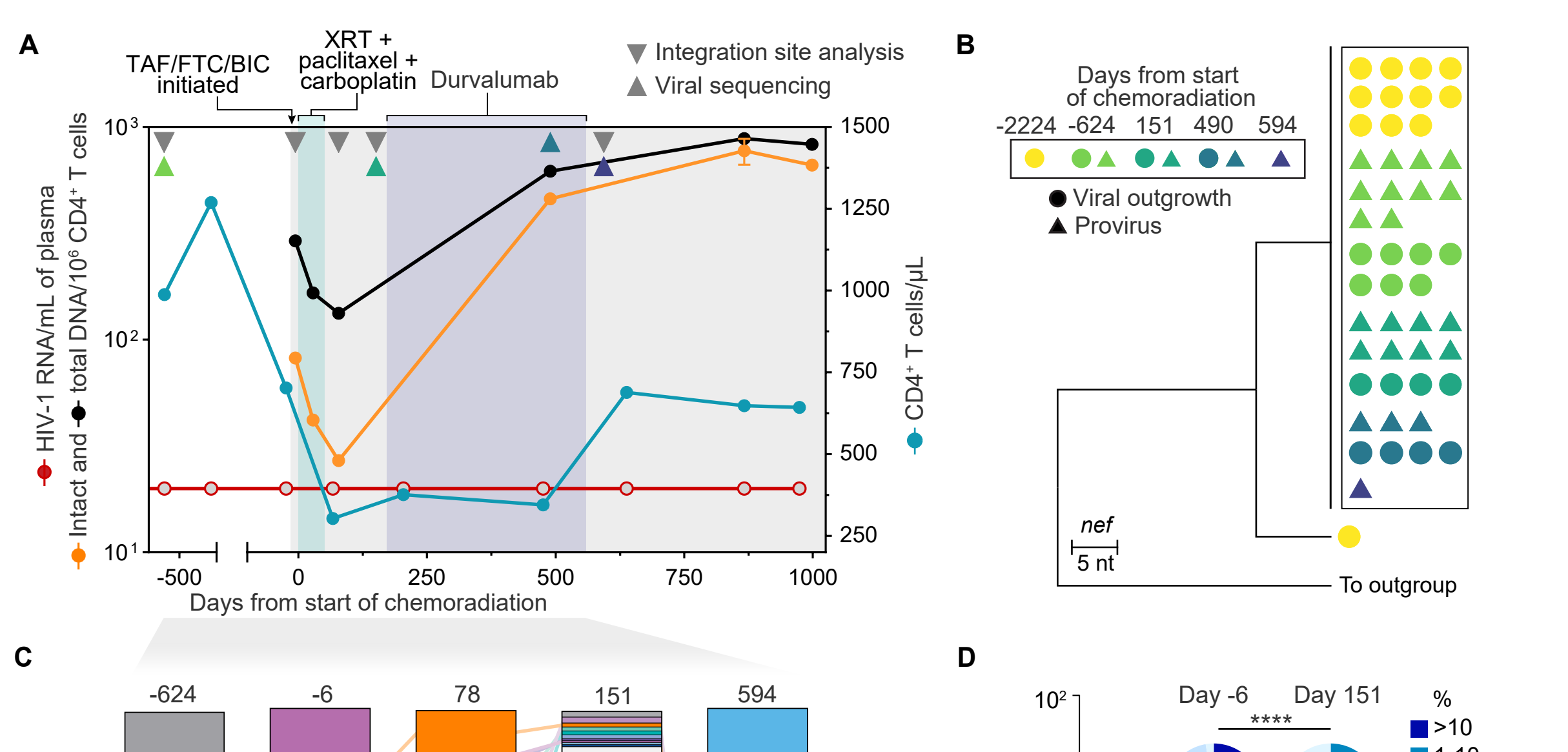

Figure 1. Chemoradiation and immunotherapy transiently affect the HIV-1 reservoir cell frequency and composition. (**A**) Clinical history of study participant ES24 before, during, and after treatment of metastatic lung cancer; values below the limit of detection are indicated with open symbols; intact and total proviruses in total CD4⁺ T cells were quantified by IPDA (orange and black, respectively); plasma HIV-1 RNA and CD4+ T cell counts are represented in red and aqua, respectively; TAF tenofovir alafenamide, FTC emtricitabine, BIC bictegravir, XRT radiotherapy. (**B**) Maximum likelihood tree of *nef* sequences recovered over time from viral outgrowth assays or limiting dilution PCR from CD4⁺ T cell -derived genomic DNA; identical sequences are indicated by the black box; HXB2 was used as outgroup. (**C**) Longitudinal integration site analysis shows contraction and reconstitution of proviruses in expanded clones; total integration sites recovered in each sample are indicated below stacked bars; integrations in ZNF genes relevant in subsequent analyses are highlighted in red. (**D**) Chemoradiation perturbs CD4⁺ T cell repertoire, especially causing loss of most expanded clones; rank-abundance curves indicate distribution of clonality among the top 250 TCRβ sequences; pie charts indicate distribution of clonotypes based of relative abundance; significance of differences between the two time points was assessed by chi-square test.

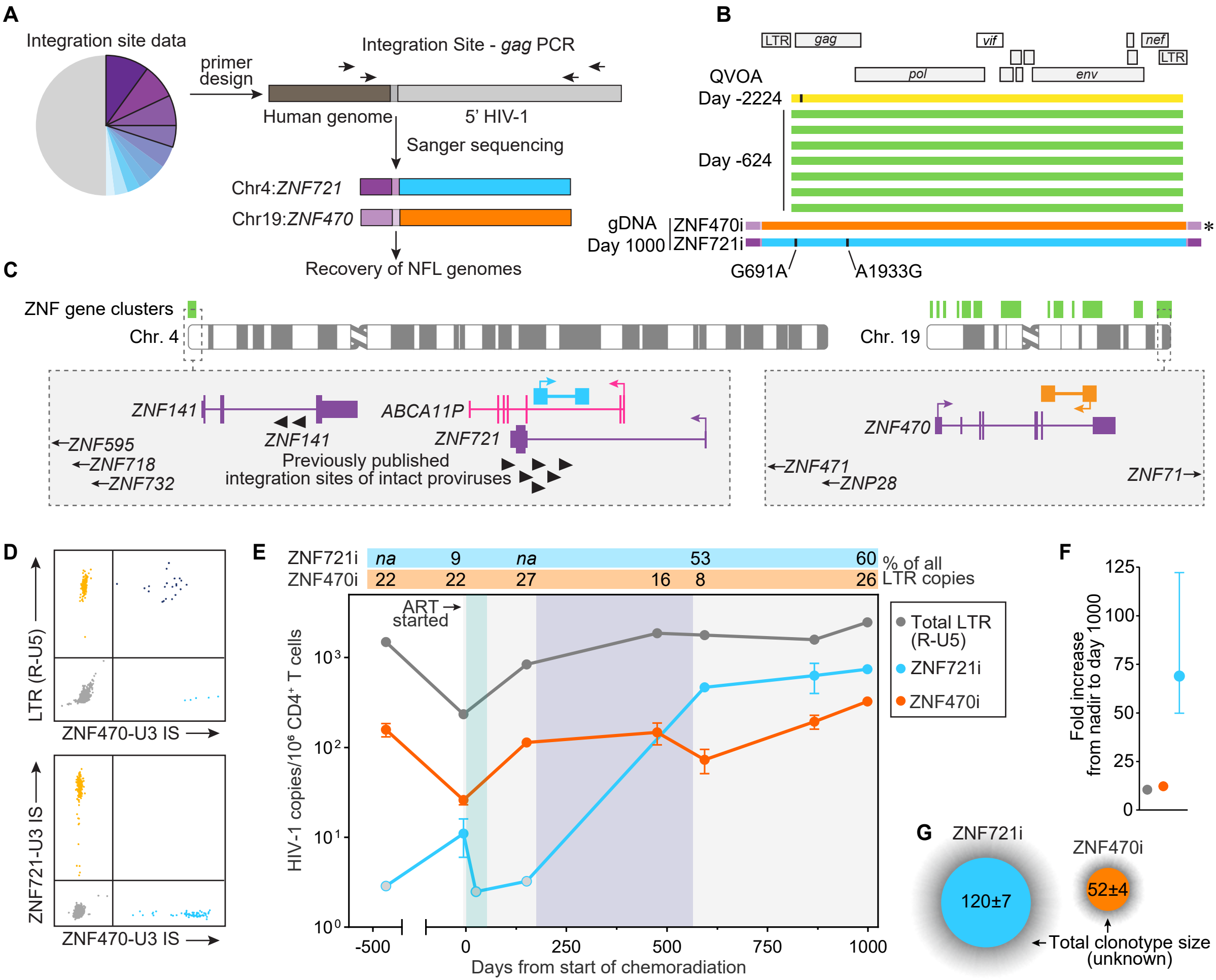

Figure 2. Persistence and expansion of two clones carrying intact proviruses integrated in Zinc Finger genes.
(**A**) Experimental approach used to match integration site and proviral sequences of interest; (**B**) Near full-length genome sequences from viral outgrowth isolates and intact proviruses integrated into *ZNF721* and *ZNF470* genes; black ticks show nucleotide differences from ZNF470i, indicated by the asterisk symbol; mutations in ZNF721i relative to ZNF479i are indicated with their positions relativo to HXB2. (**C**) Genomic location and relative orientation of intact proviruses of interest; purple tracks indicate protein coding genes, the psudogene ABCA11P is indicated in pink; black arrow heads indicate previously published integration sites; genes located outside of the grey box are highlighted with arrows; (**D**) Representative 2D dPCR plots showing duplex amplification of total LTR R-U5 copies and proviruses of interest by integration site-specific assays; (**E**) Longitudinal quantification of ZNF721i and ZNF470i proviruses before, during, and after treatment; the grey, green and purple shaded area indicate ART, chemoradiation, and immunotherapy, respectively, as in Figure 1A; open circles indicate values below the limit of detection; error bars indicate standard error of the mean; values above the graph area represent the percentage of proviruses of interest among all LTR R-U5 copies; (**F**) Fold increase of total LTR and proviruses of interest from day -6 to day 1000 from the start of chemoradiation (**G**) Estimates of total-body clone size, espressed as million cells; the shaded grey area represents the unfinfected fraction of each clonotype.

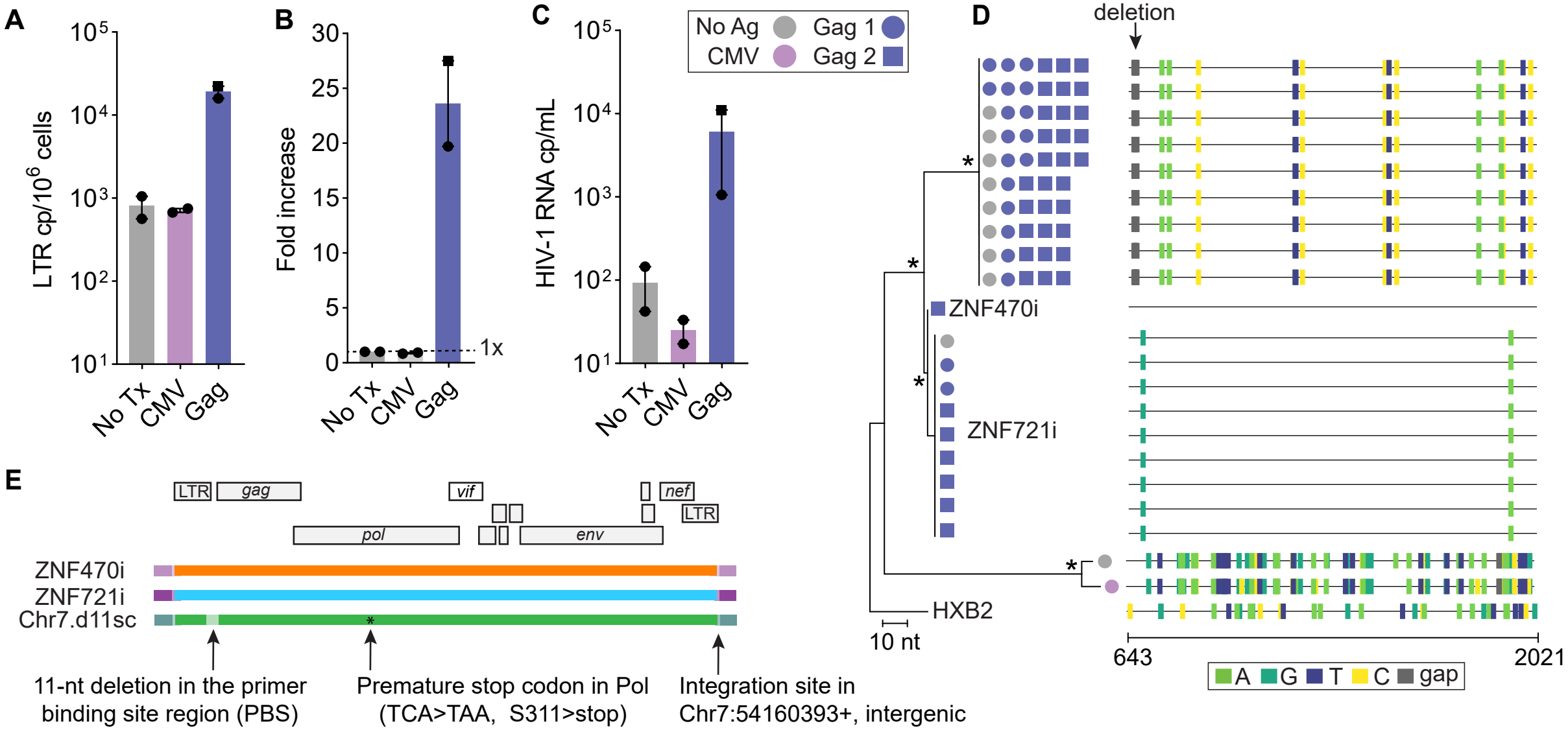

Figure 3. PBMC stimulation with HIV-1 Gag peptides induces proliferation of infected cells and virus production. (**A**) CD8-depleted PBMCs collected on day 926 post CRT were cultured for 9 days in the presence of CMV lysate, a Gag peptide pool, or left untreated (No Tx); total LTR (R-U5) copies were quantified from genomic DNA at day 9: the same Gag peptide pool wa ssued in two independent experiments from the same time point. (**B**) Stimulation with Gag peptides led to a significant fold increase in LTR copies, which was paralleled by virus production detected in the culture supernatant (**C**). (**D**) Maximum likelihood phylogeny analysis of HIV-1 RNA U5-*gag* single genome sequences; star symbols indicate node with bootstrap >75; black arrow indicates 11-nucleotide deletion; highlighter plot on the right shows nucleotide mutations relative to ZNF470i. (**E**) Characterizatoin of paired full genome sequence and integration site analysis of a new near-intact variant with a premature stop codon in Pol (indicated by asterisk). (**F**) Design of two competition probes used to distinguish intact U5-PBS from the Chr7.d11sc variant; the panel at the bottom shows a digital PCR 2D plot of a sample containing both targets. (**G**) HIV-1 DNA copies per million cells from day 9 of culture by measuring ZNF470i, ZNF721i or the 11-nt deletion from Chr7.d11.sc; numbers above bar charts indicate fold-change from No Tx. (**H**) HIV-1 RNA copies per mL of supernatant at day 9 of culture; symbols represent two independent stimulations; error bars indicate standard deviation.

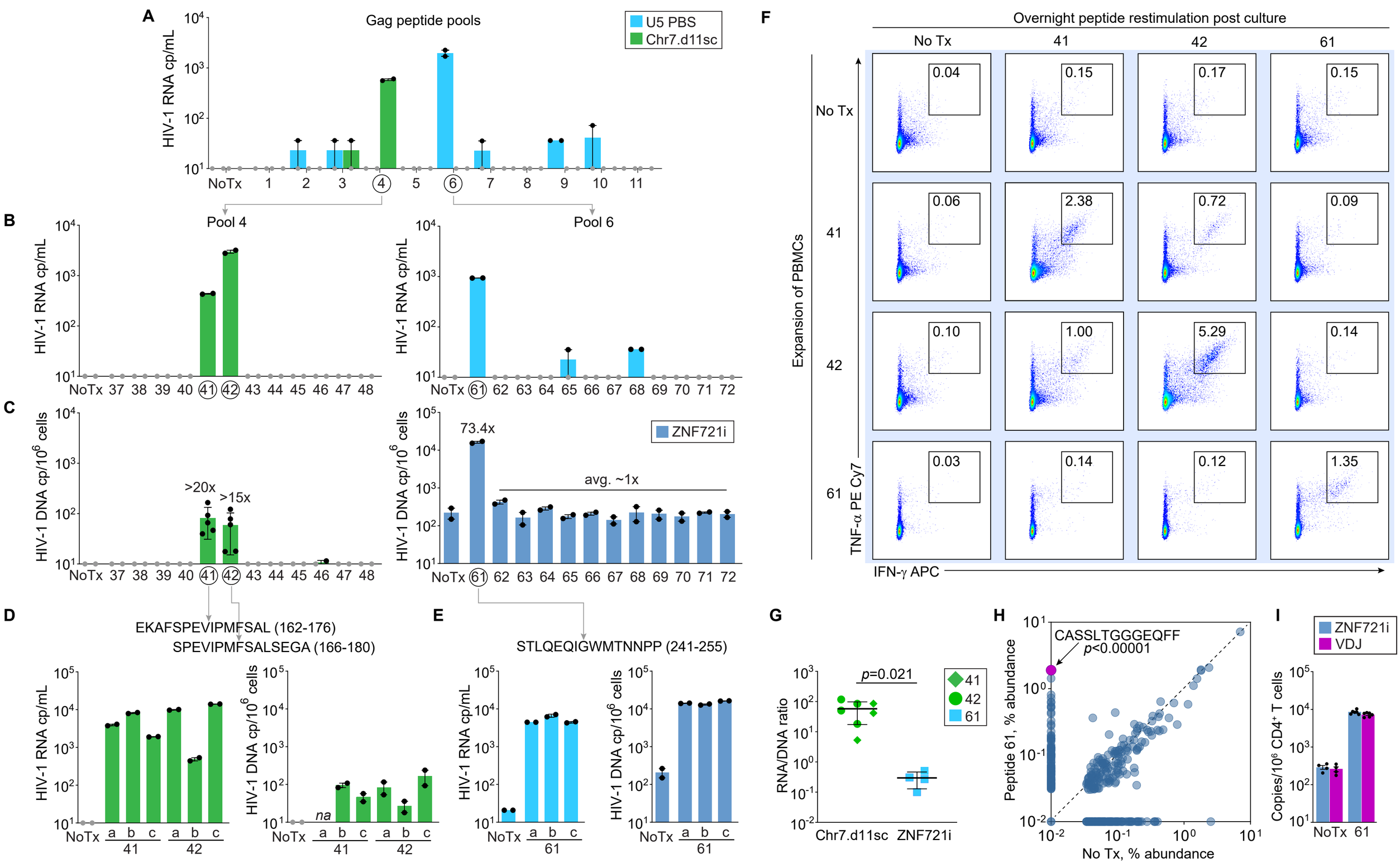

Figure 4. PBMC stimulation with HIV-1 Gag peptides induces proliferation of infected cells and virus production. (**A**) CD8-depleted PBMCs from day 1111 post CRT were stimulated with 11 mini-pools, each containing 12 Gag peptides; No Tx indicates no treatment negative control; black dots indicate technical replicates of day-9 HIV-1 RNA measurement in supernatant. (**B**) Virus production at the end of culture of CD8-depleted PBMCs from day 1142 post CRT with individual epitopes from mini-pools showing virus production in (**A**). (**C**) Frequency of proviruses of interest by day-9 of culture; fold increase compared to no treatment is indicated above each bar; peptides with increased virus production and cell proliferation are indicated below the graph. (**D** and **E**) Validation experiments with individual peptides in triplicate. (**F**) Intracellular cytokine staining of CD4⁺ T cells re-stimulated with Gag peptides of interest after PBMC expansion; numbers within gates indicate the percentage of cells positive for both TNFα and IFNγ (**G**) Differential inducibility between proviruses of interest upon stimulation with cognate Gag peptides; inducibility is expressed as the ratio between HIV-1 RNA copies in the supernatant and proviral copies in cells at the end of culture. (**H**) Analysis of differential abundance (%) of the top 1000 productive TCRs between no treatment and stimulation with peptide 61; the differential abundance of the clonotype carrying the ZNF721i provirus (CASSLTGGGEQFF) was tested by chi-square test. (**I**) Frequency of both provirus and VDJ rearrangement belonging to the CASSLTGGGEQFF clonotype in CD4⁺ T cells at the end of culture.

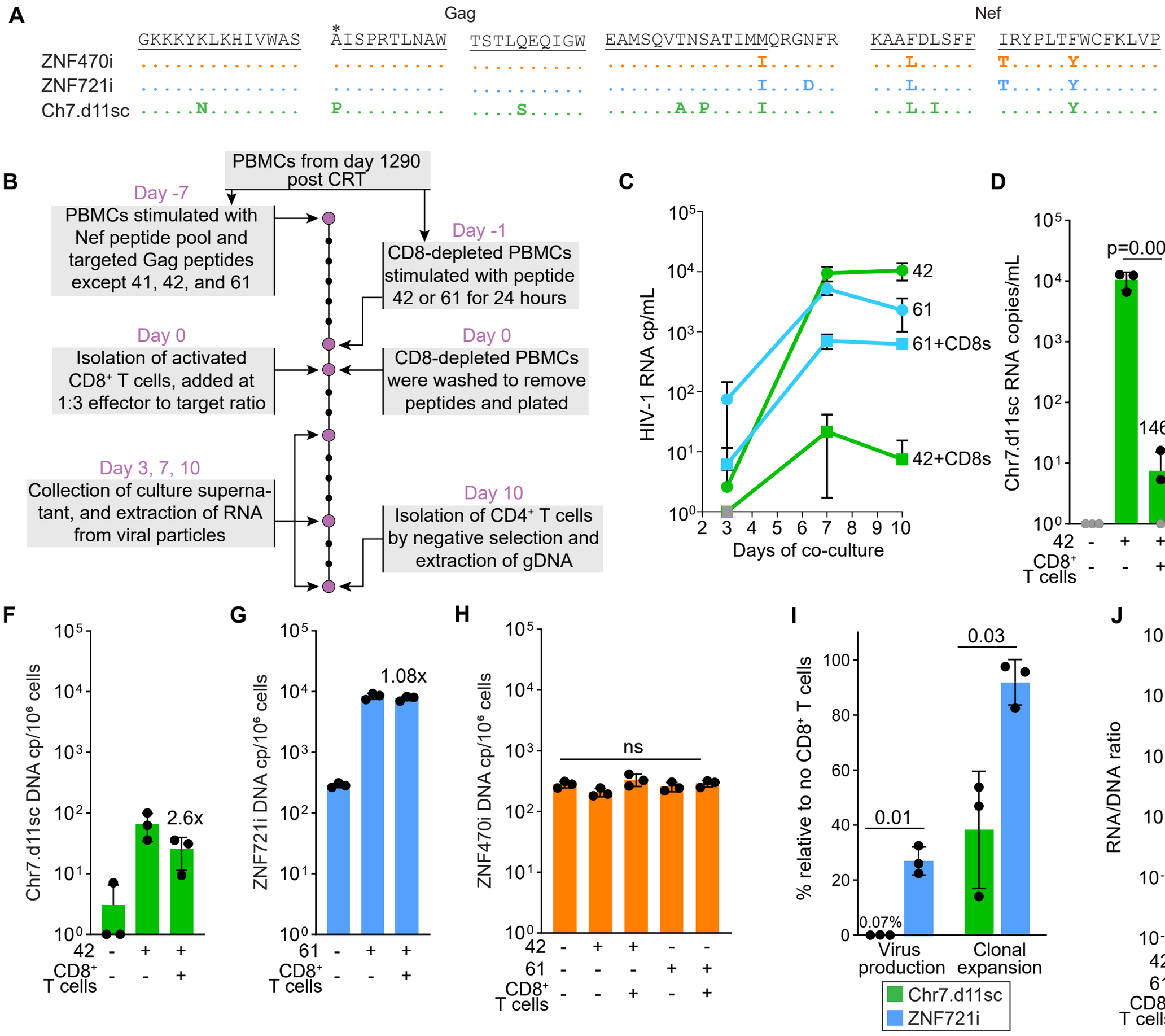

Figure 5. Differential impact of autologous CD8⁺ T cells on virus production and cell proliferation. (**A**) Analysis of escape mutations in Gag and Nef in the proviruses of interest; black lines indicate sequences recognized by CD8⁺ T cells in the context of HLA-B*57; asterisk marks an amino-acid residue involved in epitope processing that if mutated contributes to escape; full-length protein sequences are shown in Supplemental Figures S8 and S9. (**B**) Experimental design to test the impact of CD8⁺ T cells on virus production and proliferation of infected cells; aliquots of PBMCs from day 1290 post CRT were used to generate anctivated CD8⁺ T cells and, separately, stimulated CD8-depleted PBMCs with peptide 42 or 61 (**C**) HIV-1 RNA from culture supernatant at day 3, 7, and 10; symbols indicate the average of three replicate wells, error bars indicate standard deviation; fold reduction between conditions without and with CD8⁺ T cells is indicated. (**D and E**) HIV-1 RNA at day 10 across different conditions; black symbols represent replicate wells; values below the limit of detection are indicate din grey; bars show average and standard deviation. (**F-H**) Quantification of proviruses of interest measured by dPCR targeting either the 11-nucleotide deletion (Chr7.d11sc) or integration sites (ZNF721i and ZNF470i) expressed as copies per million CD4⁺ T cells. (**I**) Impact of immune recognition on virus production and proliferation of infected cells, expressed as percentage relative to wells without CD8⁺ T cells (**J**) RNA to DNA ratios of Chr7.d11sc and ZNF721i upon stimulation with cognate peptides with or without CD8⁺ T cells. The statistical differences between conditions were tested by parametric t-test.